Tensile Behavior of Polypropylene Blended with Bimodal Distribution of Styrene-Ethylene-Butadiene-Styrene Particle Size

Hiroyuki Mae,[1] Masaki Omiya,[2] Kikuo Kishimoto[3]

[1]*Honda R&D Co., Ltd., 4630 Shimotakanezawa, Haga-machi, Haga-gun, Tochigi 321-3393, Japan*
[2]*Department of Mechanical Engineering, Keio University, Kanagawa 223-8522, Japan*
[3]*Department of Mechanical and Sciences Engineering, Tokyo Institute of Technology, Tokyo 152-8552, Japan*

Received 30 May 2007; accepted 5 October 2007
DOI 10.1002/app.27482
Published online 3 December 2007 in Wiley InterScience (www.interscience.wiley.com).

ABSTRACT: The objective is to characterize the effects of the bimodal distribution of rubber particles and its blend ratio on the mechanical properties of the thermoplastic polypropylene blended with two different styrene-ethylene-butadiene-styrene triblock copolymer at the intermediate and high strain rates. Tensile tests are conducted at the nominal strain rates from 3×10^{-1} to 10^{2} (1/s). Phase morphology is investigated to estimate the bimodal rubber particle size distribution. In addition, the *in situ* observation is conducted during uniaxially stretching within transmission electron microscopy step by step to investigate the deformation events depending on the elongation of samples. The elastic modulus increased gradually as the blend ratio of large rubber particle increased. An increase in the rupture strain and the strain energy up to failure was found for the bimodal rubber particle distributed blend system where the blend ratios of small rubber particle and large rubber particle were same. This is because the smaller particles dominant blend systems show the bandlike craze deformation while the localized plastic deformation is taken place in the larger particles dominated blend systems. The synergistic effect of these rubber particles gives rise to a strong increase in the ductility of these bimodal rubber particle distributed polypropylene systems. © 2007 Wiley Periodicals, Inc. J Appl Polym Sci 107: 3520–3528, 2008

Key words: mechanical properties; particle size distribution; crazing; poly(propylene); TEM

INTRODUCTION

Polymers are widely used in the fields of aerospaces, automobiles, and electric devices because of light weight, ease of molding, and resistance to corrosion. Especially in the automobiles, Polypropylene (PP) has been extensively used for many applications such as interior and exterior automotive parts.[1] It is well known that the impact resistance of polymeric materials can be considerably modified by the incorporation of rubber materials.[2] For PP, elastomer materials such as the ethylene-propylene copolymer, ethylene-propylene-diene terpolymer, and butadiene-styrene-acrylonitrile terpolymer were used for toughening.[3–9] The overall toughening methods and theories of PP-elastomer blends are reviewed by Liang and Li.[10]

Mechanical properties of their blends are controlled by their morphology to a great extent. For rubber toughened polymers, the shape, content, size, and size distribution of the dispersed-phase particles have major effects on mechanical properties of polymer-elastomer blends.[10–23] Van der Wal et al.[24] have investigated the effect of the rubber particle size and rubber content on the fracture behavior of PP-EPR blends. They conducted tensile and Izod impact test and concluded that the larger particles influence the impact behavior adversely since those larger particles form large cavities and relieve the volume strain in a material without introducing inhomogenities from which a fracture can initiate. In the blends of PP and styrene-ethylene-butadiene-styrene triblock copolymer (SEBS), Stricker et al.[25] studied the influence of elastomer particle size on mechanical properties and showed that the critical ligament length between SEBS particles had to be thinner than 270 nm for increasing ductility of blends.

The effect of bimodal rubber particle size distribution on the mechanical properties is the additional approach for the improvement of rubber toughening in polymers. Chen and Jan[26] have studied the fracture toughness of epoxy resin with bimodal rubber particle size distribution and suggested that the small particles toughen the shear band between large particles and the large particles induce a large-scale shear deformation in the crack front. In styrene copolymers, the usefulness of a rubber phase with a

Correspondence to: H. Mae (hiroyuki_mae@n.t.rd.honda.co.jp.).

bimodal distribution has been reported by Fowler et al.[27,28] They prepared a brittle SAN copolymer with both large (1–5 μm) rubber particles created by blending with an SBS block copolymer and addition of small (0.18 μm) rubber particles created by emulsion-made rubber particles having a PMMA graft layer. A combination of the two types of particles leaded to very significant or synergistic toughening at high total rubber content. In the case of PP toughened with bimodal distribution of rubber particle size, Premphet and Paecharoenchai[29,30] have investigated the influences of a bimodal particle size distribution of ethylene-octene copolymer (EOR) in PP matrix. They applied the concept of ligament thickness and percolation theory and calculated the critical ligament thickness of the matrix and suggested that the characteristics of rubber particles showed a significant role on impact strength improvement as the matrix ligament thickness was smaller than the critical value, 0.3–0.4 μm. Recently, PP toughened with SEBS has been extensively used for interior or exterior of the automotive parts. However, the study of PP toughened with a bimodal distribution of SEBS particles is quite few. In addition, the effect of strain rate on the tensile mechanical properties has not been extensively reported in PP toughened with a bimodal size distributed SEBS particles.

The present article describes the effect of the bimodal distribution of SEBS particle size on the tensile mechanical properties such as elastic modulus, yield stress, and rupture strain. The morphology of polymer blends was observed and the distribution sizes of the SEBS particles were analyzed by transmission electron microscopy (TEM). Tensile tests were conducted at nominal strain rates from 10^{-1} to 10^{2} (1/s). In addition, *in situ* microstructural deformation events were observed step by step during uniaxially stretching within TEM to clarify the toughening mechanism for PP toughened with the bimodal rubber particle size distribution.

EXPERIMENTAL

Materials

Isotactic polypropylene (i-PP: J-3003GV supplied by Prime Polymer, Japan) whose molecular weight M_n was about 33,000 was used as the matrix polymer in this study. It has a melt flow rate (MFR) = 30 g/10 min (230°C). The density of i-PP was 900 kg/m^3. Two types of SEBS (H1221 (SEBS A) and H1062 (SEBS B), Asahi Kasei Chemicals, Japan), were used as shown in Table I. The nominal diameter of SEBS A was 80 nm and SEBS B was 250 nm. The density of SEBS A and SEBS B was 890 kg/m^3. Thus, it is considered that the volume fraction was almost same as the weight fraction in all the blends in this study.

TABLE I
Detail of SEBS

Name	MFR (g/10 min at 230°C)	Weight ratio of Stylene/ Ethylene-Butylene (%)
H1221 (SEBS A)	4.5	12/88
H1062 (SEBS B)	4.5	18/82

Blending and sample preparation

PP and SEBS copolymers were melt-mixed in a corotating twin screw extruder (Berstorff, ZE40A), with a screw diameter of 40 mm. The temperature profile was controlled at 180, 180, 190, and 192°C from feed to die zones. The screw speed was kept constant at 200 rpm. To blend two types of SEBS in PP matrix, SEBS B and PP were melt-mixed, firstly. After that, SEBS A and PP + SEBS B were melt-mixed at the same condition as the case of SEBS B and PP. The blend ratio between SEBS A and SEBS B were 0/30, 7.5/22.5, 15/15, 22.5/7.5, and 30/0 wt %, respectively. PP toughened by rubber particles usually has about 30 wt % rubber for automotive applications. Thus, our study focuses on totally 30 wt % rubber blended PP. Then, the hot extrudate was immediately quenched in a water bath and palletized. All blends were prepared under the same conditions. The blends were injection-molded to the rectangular plate whose geometry was $150 \times 150 \times 3$ mm^3. The temperature profile from the barrel to die was 200, 200, 190, and 180°C and the mold temperature was 45°C. Finally, all tensile test specimens were cut out of the plates such that the tensile direction was same as the injection direction.

Tensile test

ASTM dumbbell shape (parallel portion width 4.8 mm) micro tensile test specimens are used for measuring the stress–strain relationship (ASTM D1708). Figure 1 shows the shape of the test specimen. The thickness of test specimen is 3.0 mm. This study uses a servohydraulic high-speed impact test apparatus (Shimazu EHF U2H-20L: maximum tensile speed 15 m/s) to obtain mechanical characteristics under medium to high speed deformation. The nominal strain and nominal strain rate were calculated from the clamping distance of the test specimen where the gauge length was 22.2 mm. The nominal strain rate ranges from 10^{-1} to10^{2} (1/s). Fracture surface was observed by scanning electron microscopy (SEM: HITACHI S-4300SE/N).

Morphological investigation and *in situ* observation of deformation process

Transmission electron microscope (JEM 4000 FX (JEOL)) operating at 400 keV was used to observe the phase morphology. After staining of samples with OsO_4, ultra-thin sections were sliced by ultra

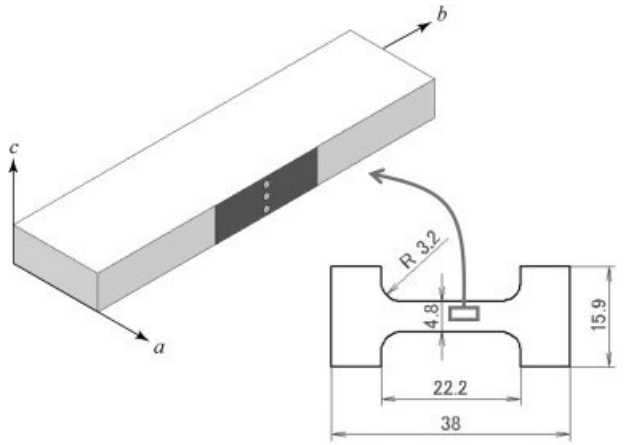

Figure 1 ASTM tensile test specimen and cutting location of thin specimen.

microtome equipped with diamond knife. In this study, three blends (SEBS A/SEBS B = 7.5/22.5, 15/15, and 22.5/7.5) were observed by TEM.

For observation of *in situ* deformation process, the samples were taken from the part of specimen including small holes whose diameter were about 30 μm made by Razor drilling (black marked in Fig. 1). In Figure 1, the *b*-axis is parallel to the injecting direction. The thin sections for *in situ* TEM were sliced with the thickness of 300 nm by means of ultra microtome equipped with a diamond knife. The thin sections were fixed on a hole of about 1 mm by two adhesive metal-tapes before being clamped by small bolt jointed plates. Then, to allow deformation of free-standing sample, the both clamping locations of metal-tape are cut before loading. Thin sections with 300-nm thickness were uniaxially stretched by single tilt straining holder (Gatan, 654) within TEM step by step to investigate the deformation events. Based on the microstructural observation during stretching, one can understand the quasistatic deformation process. It is expected that the microstructural deformation observed by TEM investigation during stretching might be same deformation mechanism as that at the deformation rate which is slower than the ductile-brittle transition deformation rate. According to the experimentally obtained tensile stress–strain relationships, the ductile fracture mode is dominant for the strain rates treated in this study. Thus, it is expected that TEM observation can be representative of the microstructural deformation mechanism.

RESULTS AND DISCUSSION

Morphology of PP/SEBS blends

Figure 2(a–c) shows the morphology of the representative PP/SEBS A/SEBS B blends where a two-phase morphology is clearly seen. Figure 2(a) is the morphology of the blends (SEBS A/SEBS B = 22.5/7.5 wt %) while Figure 2(b) is that of the blend (SEBS A/SEBS B = 15/15 wt %). Figure 2(c) shows the morphology of the blend (SEBS A/SEBS B = 7.5/22.5 wt %). SEBS particles are dispersed randomly in the PP matrix. Figure 3(a–c) shows the histograms of the rubber particle sizes measured by image analyses. In the image analysis, the commercial based software (Azo-kun, Asahi Kasei Engineering, Japan) was used. Each rubber particle was approximated as a circle and then the diameter of each circle was collected manually in the software because they could not be identified by the threshold of the black-white images. As shown clearly, all three compositions show a bimodal distribution of the rubber particle sizes. It appears that the small particles are dominant in Figure 3(a–c). However, these figures show the frequency of the count number of each rubber particle. In addition, the densities of SEBS A and B are almost same. Thus, if the number of each particle is calculated in the blend ratio (PP/SEBS A/SEBS B = 70/7.5/22.5), the number of SEBS A is much larger than that of SEBS B. In the blend (SEBS A/SEBS B = 22.5/7.5), the first peak of the particle diameter ranges approximately from 80 to 160 nm while the second peak of the particle diameter ranges from 180 to 280 nm. In the blend (SEBS A/SEBS B = 15/15), the particle size distributions firstly ranges from about 80 to 140 nm. The second particle distribution ranges from 200 to 250 nm. In the blend (SEBS A/SEBS B = 7.5/22.5), the first particle size distribution ranges from 80 to 200 nm while the second one ranges from 240 to 300 nm approximately. It is considered that the blending procedure where each SEBS was melt-mixed with PP respectively would work well because the particles were distributed randomly in the PP matrix. However, it was observed that the diameter of SEBS A increased and that of SEBS B decreased to some extent because some particles of both SEBS A and SEBS B were coalesced during mixing process. This consideration agrees with the experimental observation where the mean diameter of the large particles gets smaller as the blend ratio of the large particles increases. Further investigation about the mixing procedure such as another blending procedure where PP and SEBS A are mixed first and then PP + SEBS A and SEBS B are mixed will be the future work.

Tensile mechanical properties of PP/SEBS blends

Tensile tests under each condition are conducted three times. The typical stress–strain curves at the strain rate of 10 (1/s) are shown in Figure 4. It is shown that the stress reduction of the blend (PP/

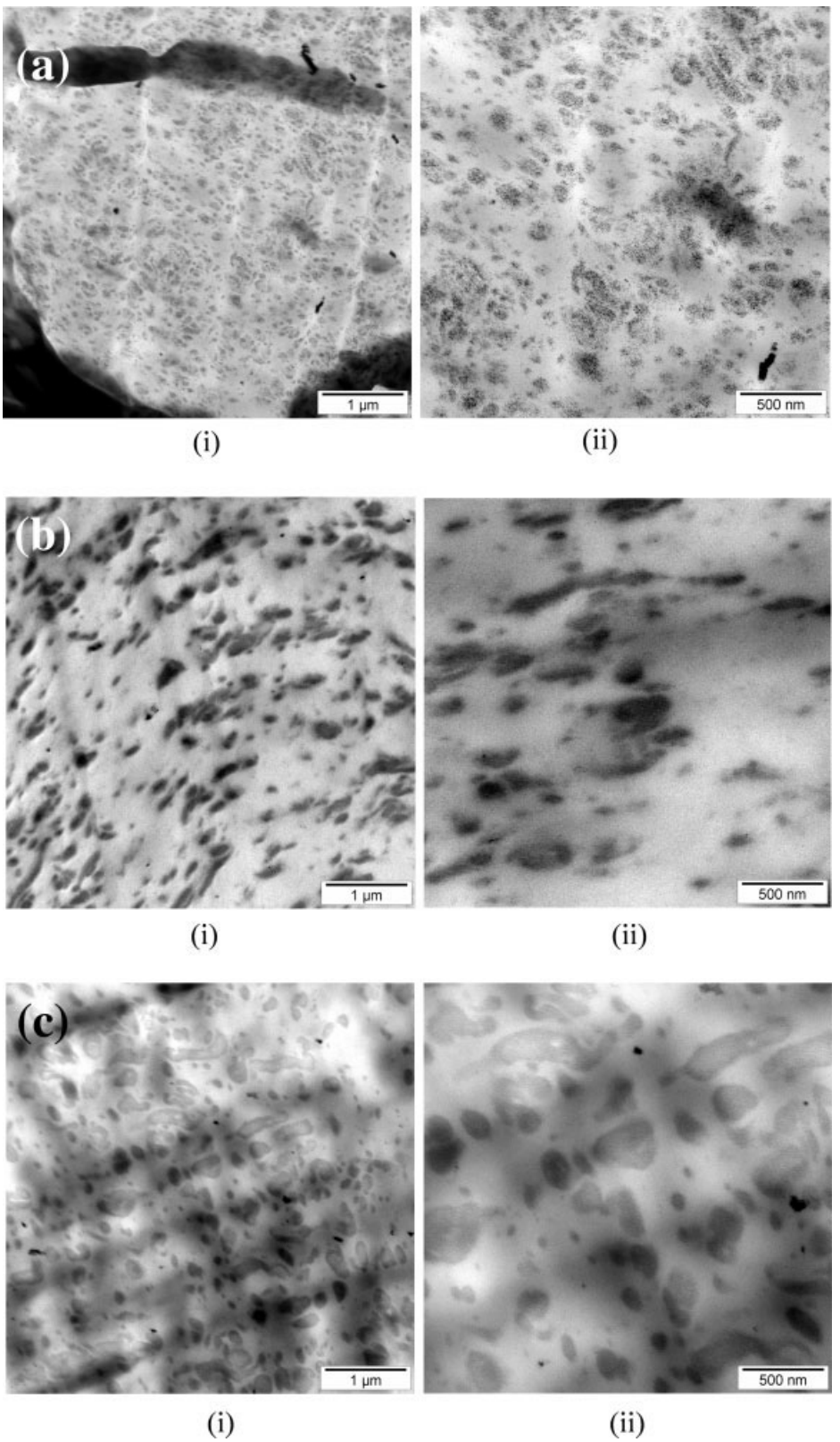

Figure 2 (a) Morphology of blend (PP/SEBS A/SEBS B = 70/22.5/7.5), (b) Morphology of blend (PP/SEBS A/SEBS B = 70/15/15), and (c) Morphology of blend (PP/SEBS A/SEBS B = 70/7.5/22.5).

SEBS A/SEBS B = 70/0/30 wt %) is the smallest while that of blend (70/30/0 wt %) is the largest. It is expected that the craze growth is different in each blend because the yield stress is almost same. Figure 5 shows the mean apparent elastic moduli calculated from three measurement data. As shown clearly, the

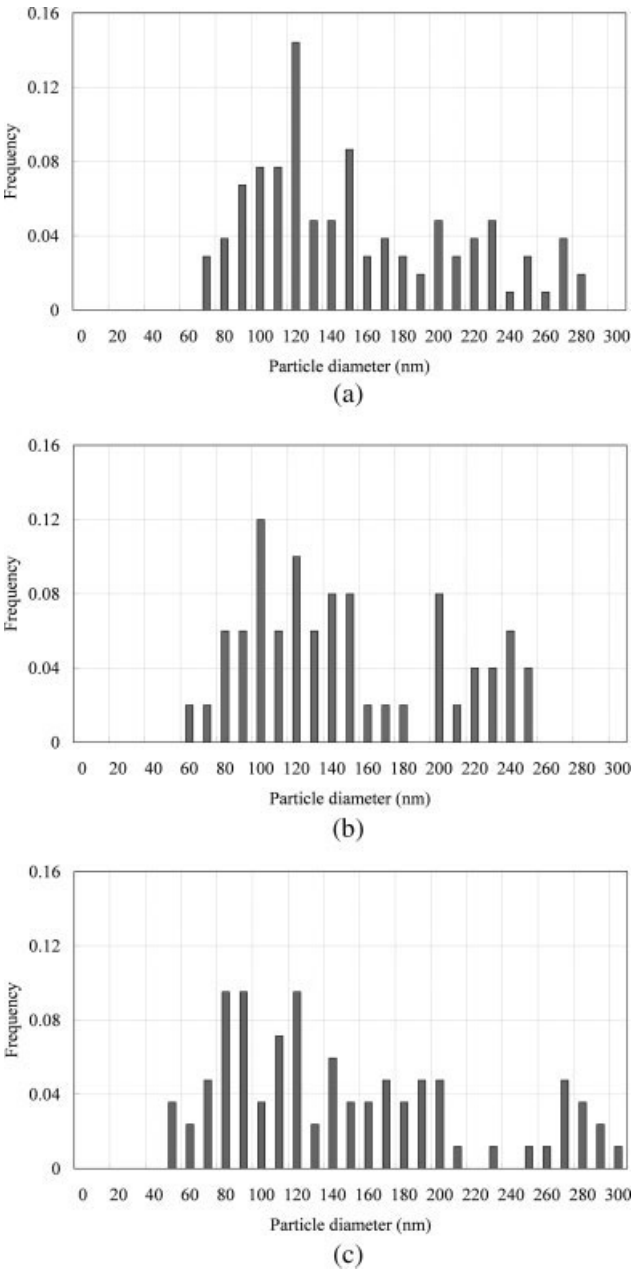

Figure 3 (a) Histogram of particle diameter of blend (PP/SEBS A/SEBS B = 70/22.5/7.5), (b) Histogram of particle diameter of blend (PP/SEBS A/SEBS B = 70/15/15), and (c) Histogram of particle diameter of blend (PP/SEBS A/SEBS B = 70/7.5/22.5).

elastic modulus increases when the blend ratio of SEBS A decreases and the blend ratio of SEBS B increases. In addition, it is observed that the strain rate dependency of the elastic modulus at the blend ratio of PP/SEBS A/SEBS B = 70/0/30 wt% is larger than that of PP/SEBS A/SEBS B = 70/30/0 wt %.

The yield stress was defined as the maximum nominal stress. In the same manner as the measurements of elastic modulus, the yield stress was measured three times at each condition and, then, the mean value is plotted in Figure 6. On the contrary to Figure 5, the yield stress shows the weak dependency of blend ratio. In addition, the strain rate dependency in all the blends is smaller than that of elastic modulus.

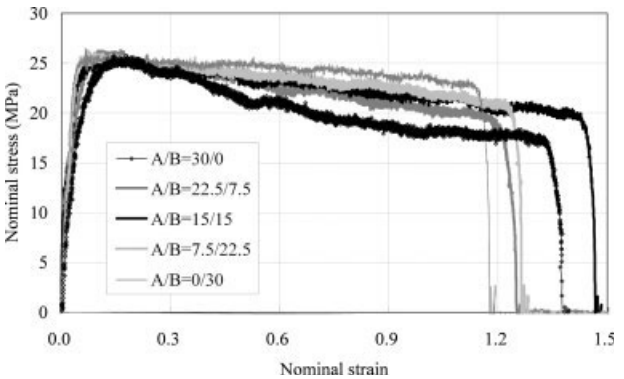

Figure 4 Typical stress–strain curves at the nominal strain rate of 10 (1/s).

Figure 7 shows the mean rupture strain plotted with the various blend ratios of SEBS B. Figure 8 shows the strain energy up to failure. The trend is similar between Figures 7 and 8. As shown clearly, the rupture strain and the strain energy up to failure have the strong dependency on the blend ratio between SEBS A and SEBS B. The sample at the blend ratio PP/SEBS A/SEBS B = 70/15/15 wt % shows the largest ductility while the sample at PP/SEBS A/SEBS B = 70/0/30 shows the smallest. It is considered that the local damage process, such as craze evolution, is different in these blends. The ductile fracture mechanism was dominant at the strain rate ranging from 0.3 to 100 (1/s).

The fracture surfaces at the nominal strain rate of 100 (1/s) are shown in Figure 9. Figure 9(a–c) shows the fracture surfaces of PP/SEBS A/SEBS B = 70/22.5/7.5, 70/15/15, and 70/7.5/22.5, respectively. As shown clearly, the ductile fracture was the dominant

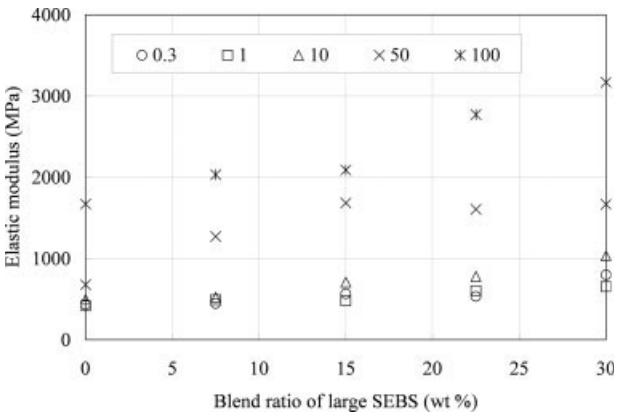

Figure 5 Effects of strain rate and blend ratio on elastic modulus.

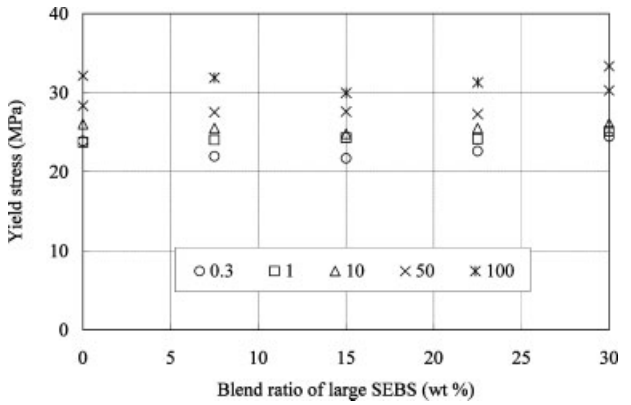

Figure 6 Effects of strain rate and blend ratio on yield stress.

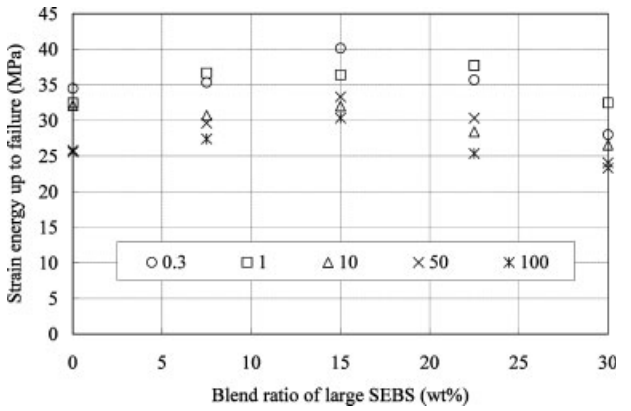

Figure 8 Effects of strain rate and blend ratio on strain energy up to failure.

mechanism at the highest strain rate in this study. Shear bands and crazes can be observed in Figure 9(a,b). In Figure 9(b), the shear bands are narrower compared to Figure 9(a). This indicates that the small SEBS particles in Figure 9(b) are easily cavitated and induce the shear deformation of the matrix. In Figure 9(c), many fibril structures are highly elongated without large deformation of the matrix. The more detail about the local damage process is discussed in the next section with the microstructural observation results.

In situ deformation processes of thin sections

Figure 10(a) shows the pictures of *in situ* deformation process taken by TEM on the blend: PP/SEBS A/SEBS B = 70/22.5/7.5 wt %. The periodical craze bands are observed on the uniaxially stretched specimen as shown in Figure 10(a). These periodical craze bands are formed in perpendicular to the direction of loading. The distance between bands are about 15 μm as shown in Figure 10(a). In addition, it is interesting that the small particles (SEBS A) are observed inside the fibrils. It is suggested that these small particles make the fibrils more ductile and enhance the rupture strain.

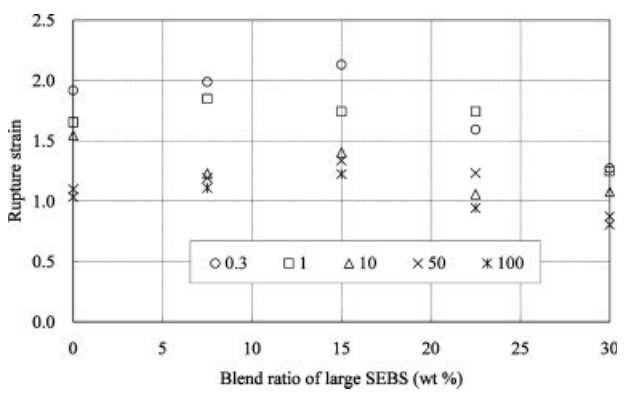

Figure 7 Effects of strain rate and blend ratio on rupture strain.

Figure 10(b) shows the pictures of *in situ* deformation process on PP/SEBS A/SEBS B = 70/15/15 wt %. Similar to the previous case, periodical craze bands are also observed on uniaxial stretched specimen. These periodical craze bands are formed in perpendicular to the direction of loading. The distance between bands are about 5 μm, which is narrower than the previous case, as shown in Figure 10(a). The number of voids is larger than that of the previous case. These voids are highly elongated to the loading direction and networklike microfibrils are formed as shown in Figure 10(b). In addition, the small particles (SEBS A) are located inside the fibrils and highly elongated. It is suggested that these deformation mechanism leads to the high elongation of this polymer blend.

Figure 10(c) shows the pictures of *in situ* deformation process on PP/SEBS A/SEBS B = 70/7.5/22.5 wt %. On the contrary to the previous cases, the length of craze bands decreases, which looks like craze spots as shown in Figure 10(c). There are a lot of large particles in this specimen, compared to the previous cases. The distance between large particles is too narrow that the small particles can not be observed inside the fibrils, leading to very short-length craze band (craze spots). The detail will be discussed in the next section.

Estimation of interparticle distances

It is well established that the interparticle distance (ID) between dispersed particles plays a crucial role to the mechanical properties, especially toughness, in polymer blends. Wu[31,32] proposed the concept of the critical ligament thickness that determines whether a blend will be tough or brittle. This concept has been applied to several rubber-toughened polymers, such as nylon,[31,32] PP,[33] and polyvinyl

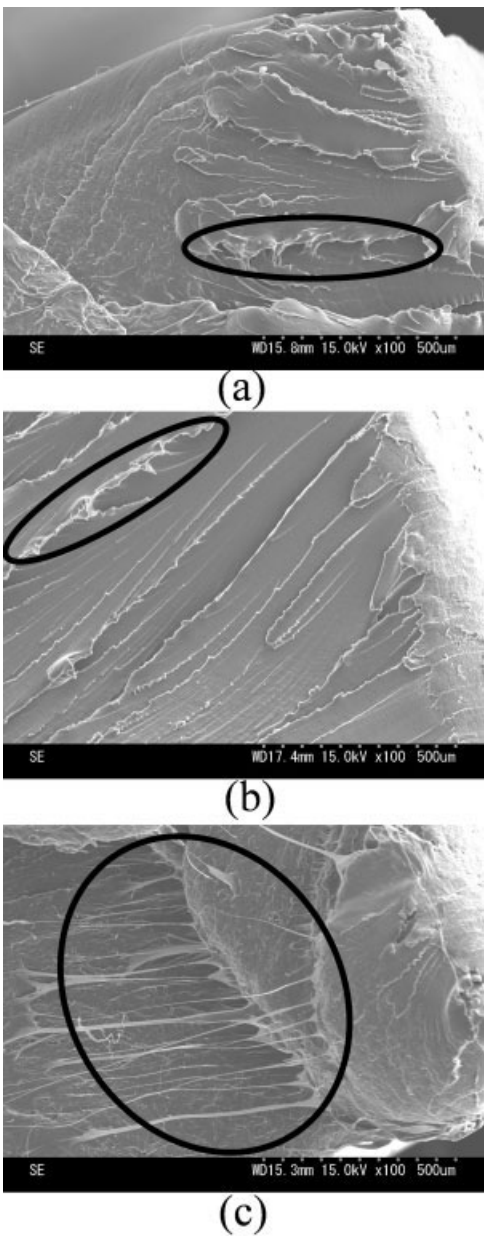

Figure 9 SEM pictures of fracture surfaces of blend (PP/SEBS A/SEBS B = (a) 70/22.5/7.5, (b) 70/15/15, and (c) 70/7.5/22.5).

chloride.[34–39] For the cubic packing of spherical particles with uniform size, the matrix ligament thickness, i.e. ID, can be obtained from eq. (1).

$$\mathrm{ID} = D\left[\left(\frac{\pi}{6\phi}\right)^{\frac{1}{3}} - 1\right], \qquad (1)$$

where, D is the rubber particle diameter and ϕ is the rubber volume fraction. At the average particle diameter D, it is clear that the ID decreases as the particle volume fraction increases. Based on the concept of stress concentration, the stress fields induced by both large and small particles can interact in all bi-

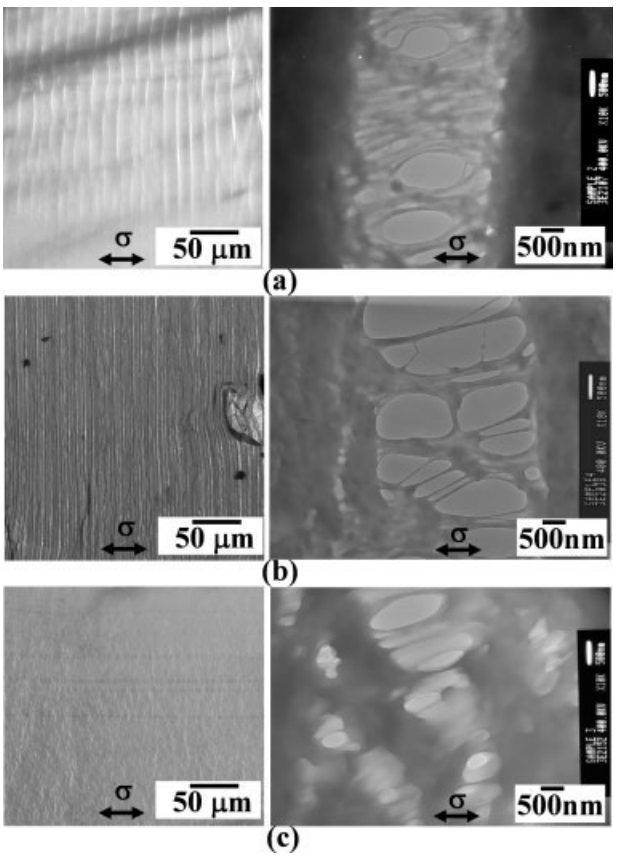

Figure 10 *In situ* deformation process of blend (PP/SEBS A/SEBS B = (a) 70/22.5/7.5, (b) 70/15/15, and (c) 70/7.5/22.5).

modal systems. It is well known that small particles cavitate and help to form the shear yielding of the matrix. The large particles are strongly related to craze formation.[31] Therefore, we focus on the ID of large particles. Table II shows the IDs of large particles calculated from eq. (1), which is assumed that only large particles would be located in the matrix. Also, the IDs of large particles are directly measured from TEM images by image analyses. The calculated results agree well with the measured results. As the ratio of large particles increases, the ID decreases and stress fields of each particle are overlapped. The stress interaction enhances the stress triaxiality, leading to craze formation easily. It is well known that the stress field interaction helps craze formation.[31] In PP toughened by EOR, the critical ID ranges from 0.3 to 0.4 μm.[30] In Table II, $\mathrm{ID}_{\mathrm{large}}$ is smaller than 0.3 μm. This means that the stress interaction occurs in our cases.

TABLE II
Estimated Interparticle Distances (unit, nm)

SEBS A/SEBS B	30/0	22.5/7.5	15/15	7.5/22.5	0/30
$\mathrm{ID}_{\mathrm{large}}$ eq.(1)	–	227.47	129.05	81.18	50.93
$\mathrm{ID}_{\mathrm{large}}$ image	–	188.6	133.3	89.4	–

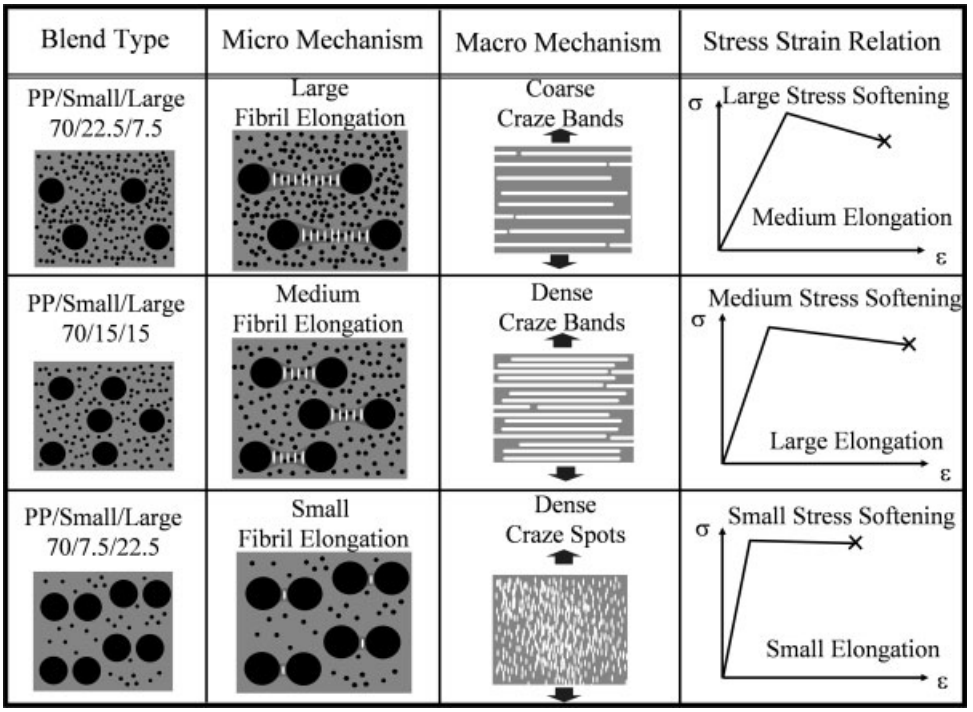

Figure 11 Toughening models of bimodal particle blends.

The summarized toughening mechanisms based on the observed results are illustrated in Figure 11. By adding small particles such as SEBS A, the small particles can be located at the ligaments between large particles (SEBS B) as shown schematically in Figure 11. Therefore, the distance of craze bands depend on the ID_{large} as illustrated in gray-color area in Figure 11. It is suggested that the small distance of craze bands should lead to large ductility. During the deformation process, small particles are located inside craze bands and enhance the ductility of each fibril such as PP/SEBS A/SEBS B = 70/15/15 wt % case. On the other hand, when the ID are smaller than the diameter of small particles such as PP/SEBS A/SEBS B = 70/7.5/22.5 wt %, small particles (SEBS A) can not be located between large particles (SEBS B) and the rupture strain does not enhance even though small particles are added as shown in Figure 11. This mechanism makes the length of craze bands very short, leading to the craze spots instead of craze bands. Therefore, the ID of large particles and the location of small particles are the key factors for improving the ductility of the bimodal polymer blends.

CONCLUSIONS

The effects of small and large SEBS particles in PP matrix on the mechanical properties at the intermediate and high strain rates were characterized. Also, *in situ* microstructural deformation events were observed within TEM. The following are the conclusions of this study:

1. The apparent elastic modulus has small morphological dependency of bimodally distributed particle size. The apparent elastic modulus decreases as the blend ratio of small particles increases. The strain rate dependency of the apparent elastic modulus increases as the blend ratio of large particles increases.
2. The yield stress is weak dependency of blend ratio and morphology. The strain rate dependency of yield stress is smaller than that of apparent elastic modulus.
3. The absorbed strain energy has strong dependency of bimodally distributed rubber particle size in the morphology. The largest material ductility is obtained in the bimodal blend (70/15/15). During the deformation process, the small particles are located inside the fibrils and highly elongated, leading to the large ductility of this polymer blend.

Based on the results of this study, it is expected that the more precisely distributed bimodal rubber particle blend system could be more ductile even at the impact loading condition.

The authors would like to acknowledge Polymer Service GmbH Merseburg, An-Institut an der Martin-Luther-Universität Halle-Wittenberg for helping the TEM observation.

References

1. Mae, H.; Takada, K.; Takahashi, J.; Yamamoto, T. Honda R&D Tech Rev 2004, 16, 165.
2. William, G. P. Polym Eng Sci 1999, 39, 2445.
3. D'Orazio, L.; Mancarella, C.; Martuscelli, E.; Polato, F. Polymer 1991, 32, 1186.
4. Stehling, F. C.; Huff, T.; Speed, C. S.; Wissler, G. J Appl Polym Sci 1981, 26, 2693.
5. Karger-kocsis, J.; Kallo, A.; Kuleznev, V. N. Polymer 1984, 25, 279.
6. Van der Waal, A.; Nijhof, R.; Gaymans, R. J. Polymer 1999, 40, 6031.
7. Moore, E. P. Polypropylene Handbook; Hanser Verlag: Munchen, 1996.
8. Liu, Y. Q.; Kontopoulou, M. Polymer 2006, 47, 7731.
9. Qiu, G. X.; Zhang, P.; Pan, J. X.; Zhao, S. G. Polym Plast Technol Eng 2003, 42, 33.
10. Liang, J. Z.; Li, R. K. Y. J Appl Polym Sci 2000, 77, 409.
11. Jang, B. Z.; Uhlmann, D. R.; Vander Sande, J. B. Polym Eng Sci 1985, 25, 643.
12. Jang, B. Z.; Uhlmann, D. R.; Vander Sande, J. B. J Appl Polym Sci 1985, 30, 2485.
13. Margolina, A.; Wu, S. Polymer 1988, 29, 2170.
14. Holz, N.; Goizueta, G. S.; Capiati, N. J. Polym Eng Sci 1996, 36, 2765.
15. Ou, Y. C.; Guo, T. T.; Fang, X. P.; Yu, Z. Z. J Appl Polym Sci 1999, 74, 2397.
16. Molnar, S.; Pukanszky, B.; Hammer, C. O.; Maurer, F. H. J. Polymer 2000, 41, 1529.
17. Lim, J. W.; Hassan, A.; Rahmat, A. R.; Wahit, M. U. Plast Rubber Compos 2006, 35, 37.
18. Borggreve, R. J. M.; Gaymans, R. J.; Schuijer, J.; Ingen Housz, J. F. Polymer 1987, 28, 1489.
19. Speri, W. M.; Patrick, G. R. Polym Eng Sci 1975, 15, 668.
20. Dao, K. C. Polymer 1984, 25, 1527.
21. Horiuchi, S.; Matchariyakul, N.; Yase, K.; Kitano, T.; Choi, H. K.; Lee, Y. M. Polymer 1997, 38, 59.
22. Jar, P.-Y.; Lee, R.; Shinmura, T.; Konishi, K. J Polym Sci Part B: Polym Phys 1999, 37, 1739.
23. Cho, K.; Yang, J. H.; Yoon, S.; Nair, M. J Appl Polym Sci 2005, 95, 748.
24. Van der Waal, A.; Verheul, A. J.; Gaymans, R. J. Polymer 1999, 40, 6057.
25. Stricker, F.; Thomann, Y.; Mulhaupt, R. J Appl Polym Sci 1998, 68, 1891.
26. Chen, T. K.; Jan, Y. H. J Mater Sci 1992, 27, 111.
27. Fowler, M. E.; Keskkula, H.; Paul, D. R. J Appl Polym Sci 1987, 28, 2145.
28. Fowler, M. E.; Keskkula, H.; Paul, D. R. J Appl Polym Sci 1988, 35, 1563.
29. Premphet, K.; Paecharoenchai, W. J Appl Polym Sci 2001, 82, 2140.
30. Premphet, K.; Paecharoenchai, W. J Appl Polym Sci 2002, 85, 2412.
31. Wu, S. Polymer 1985, 26, 1855.
32. Wu, S. J Appl Polym Sci 1988, 35, 549.
33. Jancar, J.; Dianselmo, A.; Dibenedetto, A. T. Polym Commun 1991, 32, 367.
34. Liu, Z. H.; Zhang, X. D.; Zhou, X. G.; Qi, Z. N.; Wang, F. S. Polymer 1997, 21, 5267.
35. Liu, Z. H.; Li, R. K. Y.; Tjong, S. C.; Qi, Z. N.; Wang, F. S.; Choy, C. L. Polymer 1998, 39, 4433.
36. Liu, Z. H.; Zhang, X. D.; Zhu, X. G.; Li, R. K. Y.; Qi, Z. N.; Wang, F. S.; Choy, C. L. Polymer 1998, 39, 5019.
37. Liu, Z. H.; Zhang, X. D., Zhu, X. G.; Qi, Z. N.; Wang, F. S.; Li, R. K. Y.; Choy, C. L. Polymer 1998, 39, 5027.
38. Liu, Z. H.; Zhang, X. D., Zhu, X. G.; Li, R. K. Y.; Qi, Z. N.; Wang, F. S.; Choy, C. L. Polymer 1998, 39, 5031.
39. Liu, Z. H.; Zhang, X. D.; Zhu, X. G.; Qi, Z. N.; Wang, F. S.; Li, R. K. Y.; Choy, C. L. Polymer 1998, 39, 5047.